



## GAC@Fe<sub>3</sub>O<sub>4</sub>, LDHs@Fe<sub>3</sub>O<sub>4</sub> and GO@Fe<sub>3</sub>O<sub>4</sub> applied for tetracycline hydrochloride removal in three-dimensional heterogeneous electro-Fenton process

Dandan Lv, Yan Wang, Hui-qiang Li\*

College of Architecture and Environment, Sichuan University, Chengdu 610065, China, Tel. +8618980668020; emails: lhq\_scu@163.com (H.-q. Li), 2396805935@qq.com (D. Lv), 1317466112@qq.com (Y. Wang)

Received 21 May 2020; Accepted 17 October 2020

### ABSTRACT

Tetracycline hydrochloride (TC-HCl) was harmful to human as well as ecology due to its persistence. Layered double hydroxides (LDHs), granular activated carbon (GAC) and graphene oxide (GO) were selected as the catalyst supporting materials for the three-dimensional heterogeneous electro-Fenton (3D-EF) process. The three materials were then used to prepare catalyst particles of GAC@Fe<sub>3</sub>O<sub>4</sub>, LDHs@Fe<sub>3</sub>O<sub>4</sub> and GO@Fe<sub>3</sub>O<sub>4</sub> to degrade TC-HCl. The characterizations of the LDHs@Fe<sub>3</sub>O<sub>4</sub> (8:2) particles were done by X-ray diffraction, Fourier transform infrared spectroscopy, scanning electron microscopy, energy-dispersive X-ray spectroscopy, X-ray photoelectron spectroscopy and Brunauer–Emmett–Teller. At pH of 3, the proper ratio of supporting materials (LDHs, GO, GAC) to Fe<sub>3</sub>O<sub>4</sub> improved the removal efficiency of TC-HCl. GAC@Fe<sub>3</sub>O<sub>4</sub> (8:2), LDHs@Fe<sub>3</sub>O<sub>4</sub> (8:2) and GO@Fe<sub>3</sub>O<sub>4</sub> (2:8) obtained better performance, LDHs and GO used as supporting material had better performance than GAC. Further study on the effect of different pH values showed that the LDHs@Fe<sub>3</sub>O<sub>4</sub> (8:2) acquired the highest chemical oxygen demand (COD) removal efficiency (63.03%) at pH of 7. LDHs@Fe<sub>3</sub>O<sub>4</sub> (8:2) and GO@Fe<sub>3</sub>O<sub>4</sub> (2:8) obtained similar COD removal efficiencies at pH of 3. The percentage of Fe<sup>2+</sup> leaching to solution was 2% for the LDHs@Fe<sub>3</sub>O<sub>4</sub>, which was 2.9% for the GAC@Fe<sub>3</sub>O<sub>4</sub> and 5.46% for the GO@Fe<sub>3</sub>O<sub>4</sub>. Experimental results showed that more H<sub>2</sub>O<sub>2</sub> and •OH were produced on the surface of the LDHs with pH of 7. Finally, GC-MS was used to determine the degradation pathway of TC-HCl. The LDHs had obvious advantages as catalyst supporting materials for the 3D-EF process.

**Keywords:** Tetracycline hydrochloride; Heterogeneous electro-Fenton; Hydrotalcite; Activated carbon; Graphene oxide

### 1. Introduction

Antibiotics are one of the largest drug combinations for livestock therapeutics and feed additives. Since antibiotics are poorly metabolized in the body and not easily absorbed, 30%–90% of the antibiotics remain active after excretion [1]. The abuse of antibiotics can enhance bacterial transcription. Therefore, the emergence of antibiotics worldwide has shown the urgent need to find several effective and economical methods [2]. Tetracycline hydrochloride (TC-HCl) is a kind of broad-spectrum antimicrobial agent. Due to the tenacious nature of TC-HCl, it

is difficult to remove TC-HCl by conventional wastewater treatment methods [3].

Current methods for TC-HCl removal are activated carbon adsorption, membrane technology, chemical coagulation, ion exchange, etc. [4], but these methods are often ineffective and uneconomical in treating low concentration of TC-HCl. The electrochemical advanced oxidation process (EAOP) is considered as a suitable and effective technique to achieve rapid removal and complete mineralization of persistent organic pollutants [5]. Electro-Fenton (EF) is one of the commonly used EAOP. However, homogeneous EF is still limited due to the narrow pH range. Heterogeneous

\* Corresponding author.

EF can broaden pH range, which generates a large number of hydroxyl radicals, thereby improving the electrochemical performance without the need to add any reagents [6]. With the attention of scholars, catalyst particles are the core of heterogeneous EF process.

Most of the researches on the 3D-EF process are primarily focused on iron-active species and supporting materials. Some iron minerals have been selected as catalysts for the EF process because of their widespread distribution in natural soils and sediments. The common iron minerals used in the EF process are pyrite, magnetite, hematite, goethite, tungsten iron and siderite [7]. Due to wide range of sources, low prices, and good stability, magnetite composites have been considered as promising heterogeneous EF catalysts to degrade organic pollutants in wastewater. Compared with traditional iron-supported catalysts, magnetite composites have a higher ability to degrade refractory organic pollutants due to the octahedral position in the magnetite structure. The octahedral position can easily accommodate  $\text{Fe}^{2+}$  and  $\text{Fe}^{3+}$  ions, and  $\text{Fe}^{2+}$  can be reversibly redox in the same structure [8]. In addition, being separated with a simple magnet, the magnetite used as catalyst in heterogeneous EF could improve the reuse rate of magnetite and reduce the processing cost [9]. Superior supporting materials generally have the advantages of chemical inertness, high specific surface area, good adsorption capacity, liquid–solid phase separation. Supporting materials mainly include neutral organic polymers, inorganic materials, ion exchange membranes or resins, and nanoparticles. In recent years, layered double hydroxides (LDHs) have shown a potential application as a catalyst supporting material. LDHs are anionic polymetallic compounds with a layered structure. More superior properties of the LDHs include high porosity, facile synthesis, low cost and easily available [10]. Huang et al. [11] used  $\text{FeS@LDHs}$  and  $\text{Fe}_3\text{O}_4\text{@LDHs}$  as catalysts for heterogeneous Fenton-like system, and 57.54% of methoxychlor removal was achieved after 120 min. In addition to LDHs, other materials have also been used as supporting materials in the EF process and achieved remarkable performance. Graphene and activated carbon used as carbon-based materials are interesting catalyst supports due to low cost as well as textural, chemical and morphologically tunable properties, which can play a significant role during the degradation of organic pollutants. Fernández-Sáez et al. [12] synthesized N-doped graphene aerogels and further synthesized carbon– $\text{Fe}_3\text{O}_4$  catalyst, and 71% of acetaminophen removal and 51.6% of mineralization were obtained. Sun et al. [13] prepared  $\text{Fe}_3\text{O}_4/\text{TiO}_2$ /reduced graphene oxide composites as high-performance Fenton-like catalyst that decolorized dye methylene blue within 20 min.

To the best of our knowledge, there are little previous studies on exploring the effects of support types (GAC, GO, LDHs), the ratios between supporting materials and  $\text{Fe}_3\text{O}_4$  and pH of the three variables on TC-HCl removal in the 3D-EF system.

In this work, we attempted to study the TC-HCl removal efficiencies and chemical oxygen demand (COD) removal efficiencies in the influence of support types, the ratios between supporting materials and  $\text{Fe}_3\text{O}_4$  and pH. The important parameters that effect the improvement of the performance in 3D-EF system were discussed in detail.

MgAl-LDHs, GAC and GO were selected as supporting materials in the experiments. Supporting materials@ $\text{Fe}_3\text{O}_4$  in the 3D-EF were prepared by hydrothermal synthesis method. The modern characterization technologies of X-ray diffraction (XRD), energy-dispersive X-ray spectroscopy (EDS), scanning electron microscopy (SEM), X-ray photoelectron spectroscopy (XPS), Fourier transform infrared spectroscopy (FTIR) and Brunauer–Emmett–Teller (BET) were used to confirm the excellent properties of the particles with the best performance and the dynamic changes of structure and elements in the 3D-EF process. Moreover, the intermediates during the removal of TC-HCl were analyzed based on the results of GC-MS.

## 2. Materials and methods

### 2.1. Chemicals and reagents

GAC, GO,  $\text{FeCl}_3\cdot 6\text{H}_2\text{O}$ ,  $\text{FeSO}_4\cdot 7\text{H}_2\text{O}$ ,  $\text{MgCl}_2\cdot 6\text{H}_2\text{O}$ ,  $\text{AlCl}_3\cdot 6\text{H}_2\text{O}$ ,  $\text{Na}_2\text{CO}_3$ ,  $\text{Na}_2\text{SO}_4$ , 25 wt.% of ammonia solution, tetracycline hydrochloride, NaOH and  $\text{H}_2\text{SO}_4$  were of analytical grade and used as received without further purification. All the chemicals were supplied by Aladdin Industrial Corporation, Shanghai.

### 2.2. Fabrication of LDH

MgAl-LDHs were synthesized by hydrothermal method reported previously [11]. Mixed solution of 100 mL contained 0.6 M  $\text{MgCl}_2\cdot 6\text{H}_2\text{O}$  and 0.2 M  $\text{AlCl}_3\cdot 6\text{H}_2\text{O}$  was named solution A, and 100 mL mixed solution contained 0.12 M NaOH and 0.04 M  $\text{Na}_2\text{CO}_3$  was named solution B. 100 mL of distilled water was put into a 500 mL conical flask and stirred at 700 rpm. Then, solution A and solution B were dropped into the flask dropwise to make sure that the pH of the solution was around 10. After dripping, the solution was stirred for half an hour until the solution was fully mixed; the flask was sealed and put into a constant temperature water bath at 80°C for 24 h. Precipitate in solution was washed with distilled water until the pH of the rinse became neutral. Finally, precipitate was dried at 65°C and the MgAl-LDHs were obtained by centrifugation.

### 2.3. Fabrication of $\text{GAC@Fe}_3\text{O}_4$ , $\text{GO@Fe}_3\text{O}_4$ and $\text{LDHs@Fe}_3\text{O}_4$ particles

Supporting materials@ $\text{Fe}_3\text{O}_4$  were synthesized by coprecipitation method reported previously [11,12]. Supporting materials including GAC, GO, LDHs (4 g) and 100 mL water were added into 500 mL flasks and then ultrasonicated for 30 min, respectively. 250 mL mixed solution containing 2.32 g of  $\text{FeCl}_3\cdot 6\text{H}_2\text{O}$  and 1.20 g of  $\text{FeSO}_4\cdot 7\text{H}_2\text{O}$  was slowly added into the flasks at 80°C under  $\text{N}_2$  protection, followed by stirring for 10 min. Afterward, the temperature was heated up to 85°C, 25 wt.% of ammonia solution was added quickly to precipitate  $\text{Fe}^{2+}$  and  $\text{Fe}^{3+}$  for synthesis of  $\text{Fe}_3\text{O}_4$ . Then the solution was stirred for 45 min under  $\text{N}_2$  protection. After being cooled to room temperature, the precipitate was obtained by centrifugation, and washed with distilled water until the pH of the rinse became neutral, and finally dried at 65°C. The supporting materials@ $\text{Fe}_3\text{O}_4$

composites with a mass ratio of 8:2 were prepared. The composites with mass ratios of 5:5 and 2:8 were prepared by the same method. In addition, pure  $\text{Fe}_3\text{O}_4$  was prepared by the co-precipitation method as well. The chemicals used to prepare LDHs@ $\text{Fe}_3\text{O}_4$  were relatively inexpensive and easily available. In addition, LDHs and LDHs@ $\text{Fe}_3\text{O}_4$  could be prepared in batches, and the utilization efficiency of hydro-power was also greatly improved, so the LDHs@ $\text{Fe}_3\text{O}_4$  used as catalyst for the 3D-EF to remove TC-HCl was economic.

#### 2.4. Characterization

XRD (Bruker D8 Advance, Germany) analysis was performed to analyze the crystalline structure of the particle composites. The surface functional groups of the particle composites were specified via FTIR (PerkinElmer spectrum 100, USA) analysis in the range of 400–4,000  $\text{cm}^{-1}$ . The surface morphology and elemental composition of the particle composites were determined by SEM analysis equipped with an EDS analyzer (Bruker Nano, Berlin, Germany). XPS of the particle composites was carried out with a Thermo Scientific K-Alpha+ (USA) to analyze the surface composition and electronic structures. The specific surface area and pore volume of the particle composites were appraised by the Brunauer–Emmett–Teller (BET) model using ASAP 2460 (Micromeritics, USA). The pore volume and pore distribution were calculated by the Barrett–Joyner–Halenda method.

#### 2.5. Construction of the 3D-EF

This experiment only considered the effect of 3D-EF oxidation on the removal of TC-HCl. Therefore, before beginning the reaction, a preliminary experiment on the adsorption saturation of the catalyst was performed. The specific steps were that putting the catalyst into a neutral solution containing ultra-high TC-HCl, after adsorption saturation at rest, a magnet was used to suck the catalyst out. The 3D-EF system consisted of four parts: power supply, air feeder, mechanical agitator and reaction device. DXN-FAC power supply (Jiangyin Daheng Electric Co., Ltd.) was used in the apparatus. During the reaction, the air was injected into the solution by an air pump (RS-510, Shanghai Hefan Instrument Co., Ltd., China) and the flow rate was 0.1  $\text{L min}^{-1}$ . TC-HCl solution of 100  $\text{mg L}^{-1}$  was processed in a constant current of 0.3 A, with 0.05 M  $\text{Na}_2\text{SO}_4$  as electrolyte. The mechanical agitator was used with a speed of 80 rpm to ensure well mixing between the reaction solution and the catalyst particle. 500 mL of 100  $\text{mg L}^{-1}$  TC-HCl solution was adjusted to the target pH. The pH of the solution was adjusted by  $\text{H}_2\text{SO}_4$  (1 M) and NaOH (0.5 M) solutions did not exceed 1% of the total volume. Two prepared graphite electrode plates (40 mm × 60 mm × 3 mm) were placed parallelly with a fixed-plate spacing of 2.0 cm. The reaction time for each experiment was 2 h. Samples were taken from the electrolytic cell every half an hour. The collected samples were filtered. Three parallel experiments were performed for each condition.

#### 2.6. Analytical methods

The pH was monitored by a portable pH meter (Leici PHS-25, China). The residual amount of TC-HCl was

monitored by ultraviolet spectrophotometer at 357 nm. Full spectrum of remaining TC-HCl vs. reaction times was shown in supporting data (Fig. S1) – when LDHs@ $\text{Fe}_3\text{O}_4$  (8:2) was the catalyst at pH of 3; the standard curve of TC-HCl is shown in Fig. S2. Iron ion ( $\text{Fe}^{2+}$ ) concentration was measured by O-phenanthroline spectrophotometry method.  $\text{H}_2\text{O}_2$  concentration was measured by spectrophotometry method [14], and  $\cdot\text{OH}$  concentration was measured by salicylic acid probe method [15]. COD was measured according to fast-digestion spectrophotometry method [16].

### 3. Results and discussion

#### 3.1. LDHs@ $\text{Fe}_3\text{O}_4$ (8:2) characteristics

##### 3.1.1. Brunauer–Emmett–Teller

The specific surface area of the catalyst particles would affect adsorption capability. It was reported that loading Fe/Fe oxide on mesoporous materials had high adsorption performance for some pollutants [17]. To compare the specific surface area of the LDHs@ $\text{Fe}_3\text{O}_4$  composites before and after the reaction, the  $\text{N}_2$  adsorption/desorption isotherms and pore volume of the LDHs@ $\text{Fe}_3\text{O}_4$  (8:2) are shown in Figs. 1a and b. The clear hysteresis loops were observed in the two composites in Fig. 1a. According to the International Union of Pure and Applied Chemistry (IUPAC) classification [18], the hysteresis loops of the LDHs@ $\text{Fe}_3\text{O}_4$  composites corresponded to the type V adsorption isotherms. Before reaction, the BET surface area was 43.3  $\text{m}^2 \text{g}^{-1}$ , and the pore volume was 0.17  $\text{cm}^3 \text{g}^{-1}$ , and the average pore diameter was 14.57 nm. After the EF reaction, the BET surface area was 57.4  $\text{m}^2 \text{g}^{-1}$ , the pore volume was 0.18  $\text{cm}^3 \text{g}^{-1}$ , and the average pore diameter was 12.27 nm. The average pore diameter corresponded to the mesoporous pore, agreeing with the  $\text{H}_3$ -type hysteresis loops, which was caused by the presence of slit-type pores that were created from the plate-like particles characterizing the feature of the layered materials [19]. The results showed that the specific surface area and the pore volume of the LDHs@ $\text{Fe}_3\text{O}_4$  composites increased after reaction, but pore diameter decreased. The reason would be that  $\text{Fe}_3\text{O}_4$  on the surface of the LDHs@ $\text{Fe}_3\text{O}_4$  gradually decreased with the progress of the EF process. Similarly, the structure and surface morphology of the MgAl-LDHs also changed and more cracks would emerge, resulting in the increase of the specific surface area and the pore volume.

##### 3.1.2. X-ray diffraction

The XRD pattern of the LDHs@ $\text{Fe}_3\text{O}_4$  (8:2) before and after the reaction with pH of 7 is shown in Fig. 2. The phases were identified by comparing the measured patterns with the reference patterns of magnetite and LDHs from the JCPDS database ( $\text{Fe}_3\text{O}_4$  [JCPDS NO.74-0748] and MgAl-LDHs [JCPDS NO.70-2151]) [20]. In the diffraction patterns of the MgAl-LDHs@ $\text{Fe}_3\text{O}_4$ , characteristic patterns of LDHs and  $\text{Fe}_3\text{O}_4$  were observed, indicating that both phases were presented in the structure. Diffraction peaks indexed to  $\text{Fe}_3\text{O}_4$  at  $2\theta$  were 30.1°, 35.6°, 43.4° and 57.4°, which were well consistent with the previous reports, corresponding to (2 2 0), (3 1 1), (4 0 0), (5 1 1) [21]. MgAl-LDHs were also

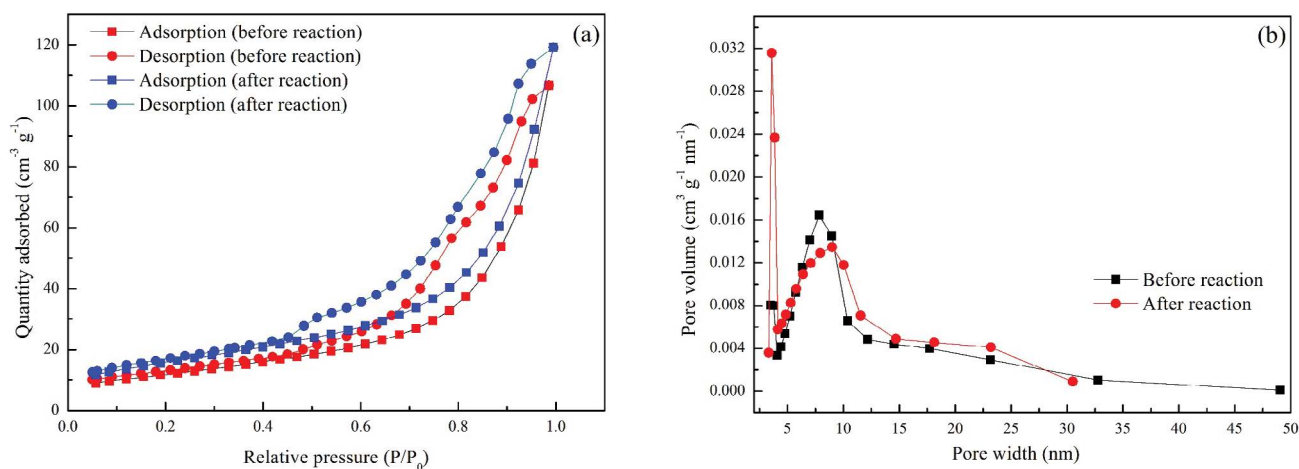


Fig. 1. BET characterization for the LDHs@Fe<sub>3</sub>O<sub>4</sub> (8:2), N<sub>2</sub> adsorption/desorption isotherms (a) and pore volume (b).

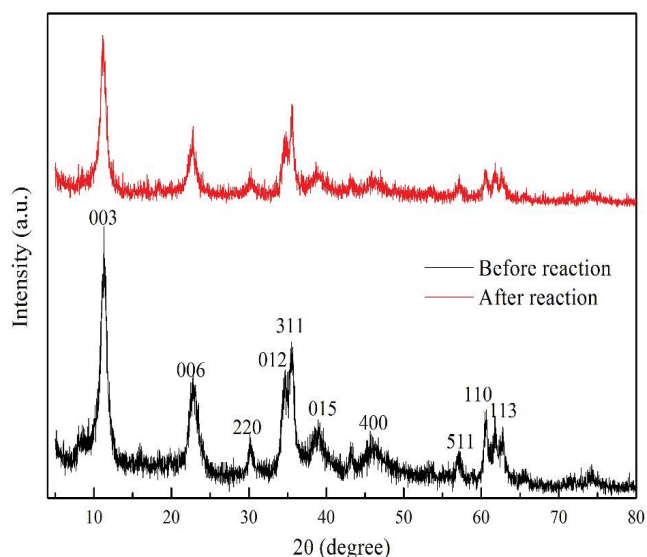


Fig. 2. X-ray diffraction of LDHs@Fe<sub>3</sub>O<sub>4</sub> (8:2).

evidenced by the characteristic peaks of 11.3°, 22.8°, 34.7°, 39.1°, 46.3° and 62.4° at 2θ, corresponding to (0 0 3), (0 0 6), (0 1 2), (0 1 5), (1 1 0) and (1 1 3), respectively [22]. The characteristic peaks of the LDHs@Fe<sub>3</sub>O<sub>4</sub> before and after the reaction were almost the same, indicating that the MgAl-LDHs@Fe<sub>3</sub>O<sub>4</sub> had excellent stability. But the intensity of the characteristic peaks before the reaction was higher than that after the reaction, which might be that the EF reaction affected the crystal structure of the MgAl-LDHs@Fe<sub>3</sub>O<sub>4</sub>. Meanwhile, the peak of (3 1 1) lattice plane had a chemical shift, which illustrated that the decrease of Fe<sub>3</sub>O<sub>4</sub> would change the interlayer spacing of the MgAl-LDHs.

### 3.1.3. SEM and EDS

The surface morphology of the LDHs@Fe<sub>3</sub>O<sub>4</sub> (8:2) was characterized by the SEM. Figs. 3a<sub>1</sub> and a<sub>2</sub> show the layered structure and spherical crystals of the LDHs@Fe<sub>3</sub>O<sub>4</sub>. In Fig.

3a<sub>2</sub>, the LDHs@Fe<sub>3</sub>O<sub>4</sub> retained its original form after the reaction, but the spherical crystals were reduced obviously. The rough porous surface of the LDHs@Fe<sub>3</sub>O<sub>4</sub> showed that the scale-like irregular and spherical crystals on the layered surface were mainly caused by the synthesis of MgAl-LDHs and Fe<sub>3</sub>O<sub>4</sub>. The Fe<sub>3</sub>O<sub>4</sub> existed on the surface of the LDHs and entered the pores of the LDHs as well, ensuring good dispersibility. The EDS micrographs of the LDHs@Fe<sub>3</sub>O<sub>4</sub>, along with corresponding quantitative results, are exhibited in Figs. 3b<sub>1</sub> and b<sub>2</sub>. Before reaction, as shown in Fig. 3b<sub>1</sub>, the atomic percentage (A%) of Mg was 3.03 times more than that of Al. Based on the Mg/Al molar ratio, the value of *x* in the common formal of MgAl-LDHs, that is, Mg<sub>1-x</sub>Al<sub>x</sub>(OH)<sub>2</sub>(CO<sub>3</sub>)<sub>*x/n*</sub>·*y*H<sub>2</sub>O was obtained to be *x* = 1/(1 + 3.03) = 0.25. Hence, the *x/n* value was calculated as 0.125, according to the *x* and *n* values of 0.25 and 2, respectively. Then, the formula of MgAl-LDHs was deduced to be Mg<sub>0.75</sub>Al<sub>0.25</sub>(OH)<sub>2</sub>(CO<sub>3</sub>)<sub>0.125</sub>·*y*H<sub>2</sub>O [23]. Mg/Al molar ratio after the reaction (Fig. 3b<sub>2</sub>) was only 1.88, indicating that some Mg and Al elements were dissolved from the LDHs@Fe<sub>3</sub>O<sub>4</sub> during the EF reaction. At pH of 3, more Mg<sup>2+</sup> and Al<sup>3+</sup> were leached and reprecipitated on the catalyst surface, and the active metal sites of the catalyst were reduced, which affected the performance of the 3D-EF system. In addition, the amount of Fe on the surface of the particle changed a little illustrating the good retention effect of the LDHs on the catalyst.

### 3.1.4. Fourier transform infrared spectroscopy

The FTIR results of the LDHs@Fe<sub>3</sub>O<sub>4</sub> before and after reaction are shown in Fig. 4. The broad peak at 3,449 cm<sup>-1</sup> was attributed to the O–H stretching mode of the layer surface and interlayer water molecules. The band at 1,635 cm<sup>-1</sup> could be assigned to the C–O bond and H<sub>2</sub>O bending vibration of the interlayer water [24]. Water molecules could also be confirmed by the presence of the band at 1,635 cm<sup>-1</sup>, which was attributed to the H–O–H deformation mode [25]. An intense absorption at 1,366 cm<sup>-1</sup> was ascribed to the asymmetric stretching of CO<sub>3</sub><sup>2-</sup> in the interlayer, indicating some CO<sub>3</sub><sup>2-</sup> ions existed in the gallery of MgAl-LDHs [26]. The weak absorption band at 1,070 cm<sup>-1</sup> was observed

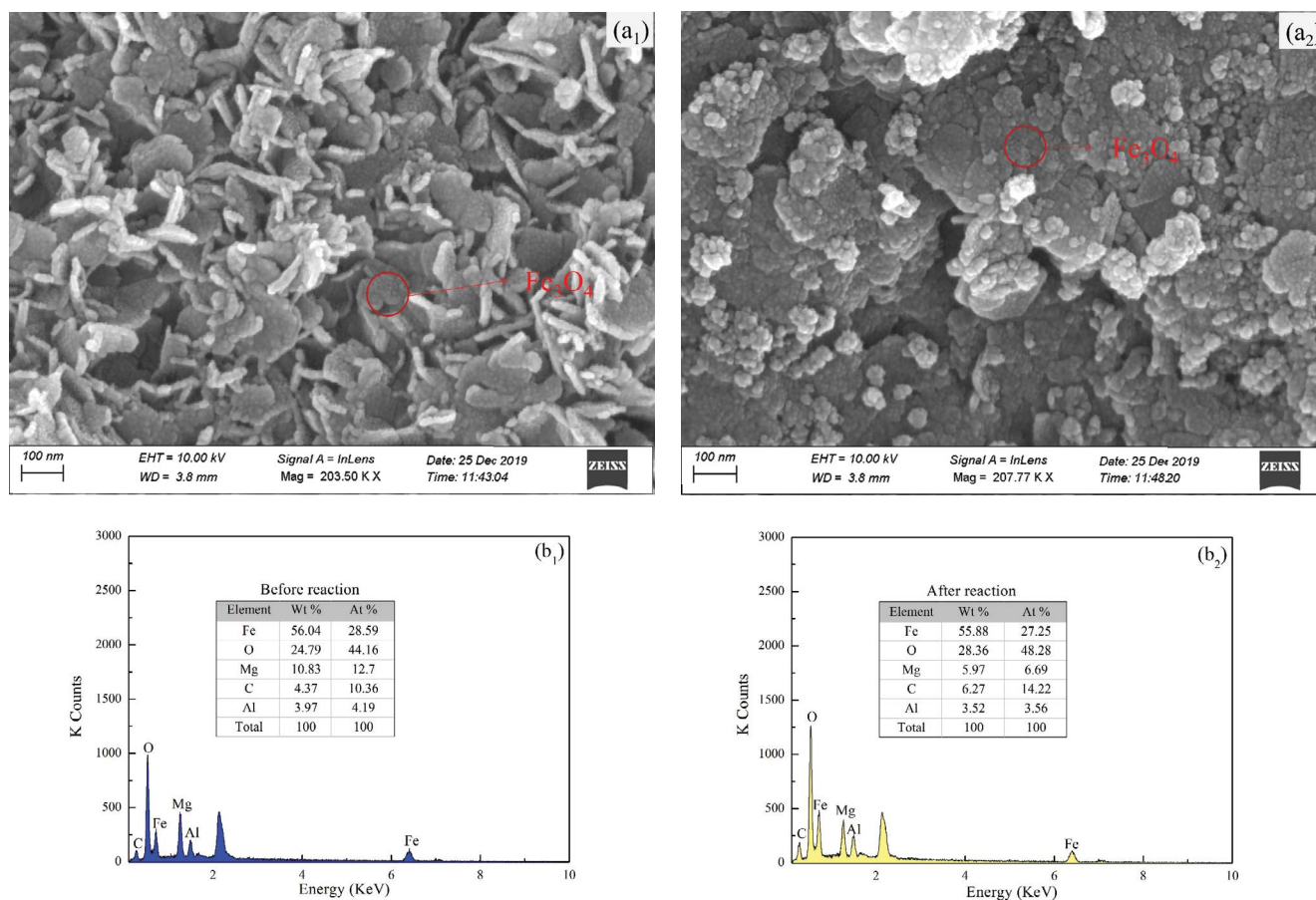


Fig. 3. LDHs@Fe<sub>3</sub>O<sub>4</sub> (8:2) characterization: SEM before reaction (a<sub>1</sub>), SEM after reaction (a<sub>2</sub>), EDS before reaction (b<sub>1</sub>) and after reaction (b<sub>2</sub>).

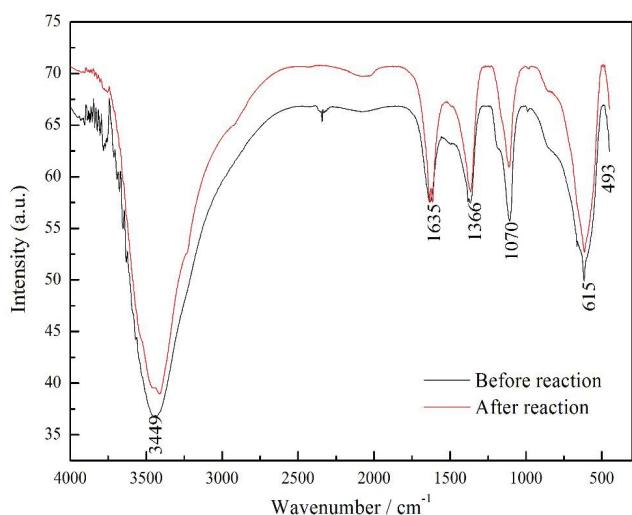


Fig. 4. Fourier transform infrared spectroscopy of the LDHs@Fe<sub>3</sub>O<sub>4</sub> (8:2).

and corresponded to stretching vibration of carbonate. The absorption bands in the range of low wave number (400–800 cm<sup>-1</sup>) were mainly caused by the Al–O, Mg–O, O–Mg–O and O–Al–O, Fe–O in the metal hydroxide sheets in

the brucite-like lattice [27]. The peaks observed at 580 cm<sup>-1</sup> could be attributed to the vibration of Fe–O from Fe<sub>3</sub>O<sub>4</sub>. Compared with the original LDHs@Fe<sub>3</sub>O<sub>4</sub>, some dominant peaks of the LDHs@Fe<sub>3</sub>O<sub>4</sub> after reaction had slight shifts. For example, the bending vibration of oxygen-containing groups slightly shifted from 1,366 to 1,363 cm<sup>-1</sup>. These observations were consistent with the results observed by XRD.

### 3.1.5. X-ray photoelectron spectroscopy

The surface chemical states of the LDHs@Fe<sub>3</sub>O<sub>4</sub> were further analyzed by XPS spectra. The survey XPS spectra show all elements of Mg, Al, C, O and Fe in Fig. 5a. The peaks at 1,304.4 and 74.4 eV before reaction (Figs. 5b and c) were assigned to the chemical elements of Mg 1s and Al 2p, respectively, which verified that Mg and Al existed as the oxide/hydroxide chemical states. It was obvious that Mg and Al shifted to higher binding energy after reaction, but changes in binding energy were small, indicating that the chemical bonds of Mg and Al did not change significantly at pH of 7. Meanwhile, as observed from Fig. 5d, the presence of C–C, C–O C=O and O–C=O was fitted by the peaks centered at 284.8, 286.4, 288.9 and 289.9 eV, indicating indirectly that the reference carbon and the presence of intercalated carbonate anions in the layered structure of

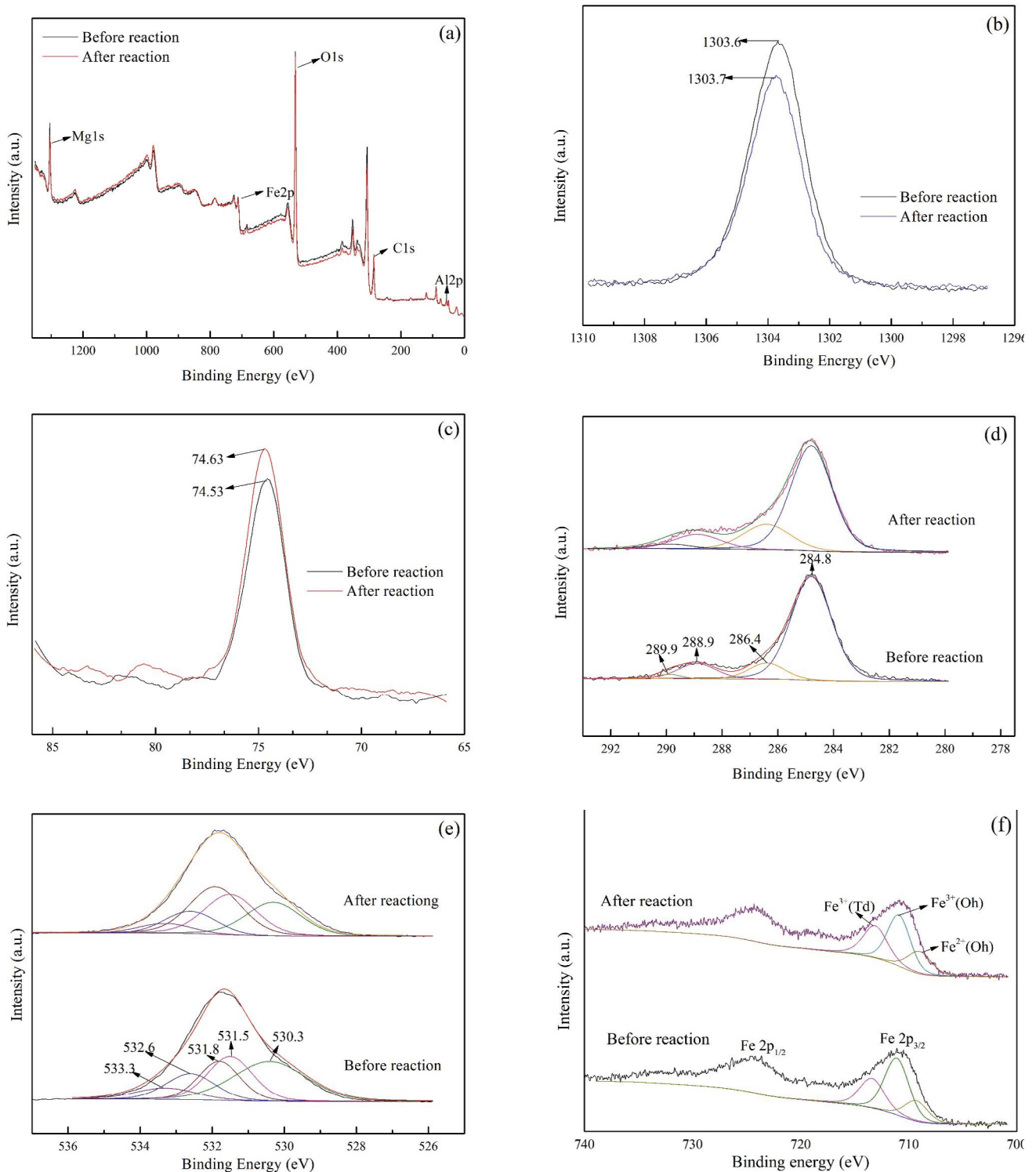


Fig. 5. X-ray photoelectron spectroscopy (XPS) characterization for the LDHs@Fe<sub>3</sub>O<sub>4</sub> (8:2): XPS survey (a), Mg (b), Al (c), C (d), O (e), Fe (f).

the MgAl-LDHs [28]. The O1s peaks in Fig. 5e were fitted with five peaks at 530.3, 531.5, 531.8, 532.2 and 533.3 eV. The two peaks at 530.3 and 531.5 eV in O1s spectrum were attributed to M–O (M was Mg, Al or Fe in this section) and metal hydroxides or hydroxyl groups [29]. The other three

peaks at 531.8, 532.2 and 533.3 eV were attributed to O–C=O, C=O and C–O. The residual peak at 532.33 eV was attributed to the chemical equivalent oxygen in the bidentate bond (O–C=O) [30]. In the Fe2p spectra (Fig. 5f), the peaks located at 710.8 and 725.1 eV of binding energy belong to Fe 2p<sub>3/2</sub>

and Fe 2p<sub>1/2</sub>, respectively, which illustrated the existence of Fe<sub>3</sub>O<sub>4</sub> in the composite. The Fe 2p core level spectra showed that the peaks of LDHs@Fe<sub>3</sub>O<sub>4</sub> before reaction at 709.3, 711 and 713.4 eV represented the Fe<sup>2+</sup> in octahedral (Oh) sites, Fe<sup>3+</sup> in octahedral (Oh) sites, and Fe<sup>3+</sup> in tetrahedral (Td) sites [31]. The peak located at 709.3 eV shifted to 709 eV for Fe<sup>2+</sup> (Oh), and the peak at 711 eV transferred to 710.7 eV for Fe<sup>3+</sup> (Oh). The peak varied from 713.4 to 713.2 eV for Fe<sup>3+</sup> (Td), which could be attributed to the electron transfer between Fe<sup>2+</sup> and Fe<sup>3+</sup> during the removal reaction.

### 3.2. Performance of the catalyst particles

The optimum pH for traditional Fenton process was considered to be around 3 [5]. In order to analyze the influence of different kinds of catalyst particles on TC-HCl removal in the 3D-EF process, the experiments were carried out in the same conditions except for the different catalyst particles. The initial pH value of the 3D-EF process was adjusted at pH of 3.

TC-HCl removal performance with GAC@Fe<sub>3</sub>O<sub>4</sub> is shown in Fig. 6. When the mass ratios of GAC and Fe<sub>3</sub>O<sub>4</sub> were 2:8, 5:5 and 8:2, TC-HCl removal efficiencies were 82.58%, 83.06% and 88.89%, respectively. The 3D-EF system obtained high TC-HCl removal efficiency at different mass ratios. COD removal efficiencies with GAC@Fe<sub>3</sub>O<sub>4</sub> are shown in Fig. 7a. COD removal efficiency was 5.0% after reaction for 2 h in blank group. When pure Fe<sub>3</sub>O<sub>4</sub> was added into the system, a significant increase in COD removal efficiency was observed, COD removal efficiency after 2 h increased from 5.0% to 31.0%, 6.2 times of that in the absence of catalyst particles. COD removal efficiencies were 33.09%, 36.68%, 41.96% with GAC and Fe<sub>3</sub>O<sub>4</sub> ratios of 2:8, 5:5 and 8:2, respectively. When the proportion of Fe<sub>3</sub>O<sub>4</sub> decreased, COD removal efficiency increased gradually. The reason might be that oxygen reacted on the surface of the catalyst particles to generate H<sub>2</sub>O<sub>2</sub>, and then reacted with Fe<sup>2+</sup> to generate •OH, so the larger the specific surface area of the support materials was, the more H<sub>2</sub>O<sub>2</sub> and •OH would be generated. The concentrations of H<sub>2</sub>O<sub>2</sub> and •OH would be shown later. Another reason was that •OH generated on the surface of catalyst was consumed by excessive ferrous ions when GAC@Fe<sub>3</sub>O<sub>4</sub> was coated with too much Fe<sub>3</sub>O<sub>4</sub>. Similar trends were observed by Wang et al. [32]. Obviously, GAC@Fe<sub>3</sub>O<sub>4</sub> at ratio of 8:2 obtained the highest COD removal efficiency, because the content of Fe<sub>3</sub>O<sub>4</sub> coated on the surface of GAC@Fe<sub>3</sub>O<sub>4</sub> at ratio of 8:2 was the least. At the same time, the conclusion was verified by the COD removal efficiency using the pure Fe<sub>3</sub>O<sub>4</sub>. Therefore, when the initial pH value was 3, the best COD removal efficiency was achieved with the mass ratio of the GAC and Fe<sub>3</sub>O<sub>4</sub> at 8:2.

The performances of the LDHs@Fe<sub>3</sub>O<sub>4</sub> on TC-HCl and COD removal are shown in Figs. 6 and 7b. Different from the GAC@Fe<sub>3</sub>O<sub>4</sub>, TC-HCl removal efficiencies had some differences with the variation of the mass ratios between LDHs and Fe<sub>3</sub>O<sub>4</sub>, and the minimum efficiency was 81.57% with ratio of 2:8 while the maximum value was 93.28% with ratio of 8:2. COD removal efficiencies varied from 35.56% to 60.93% with the increase of mass ratio. COD removal efficiency of LDH@Fe<sub>3</sub>O<sub>4</sub> at a ratio of 8:2 was 12 times than the black group. COD removal efficiencies gradually increased

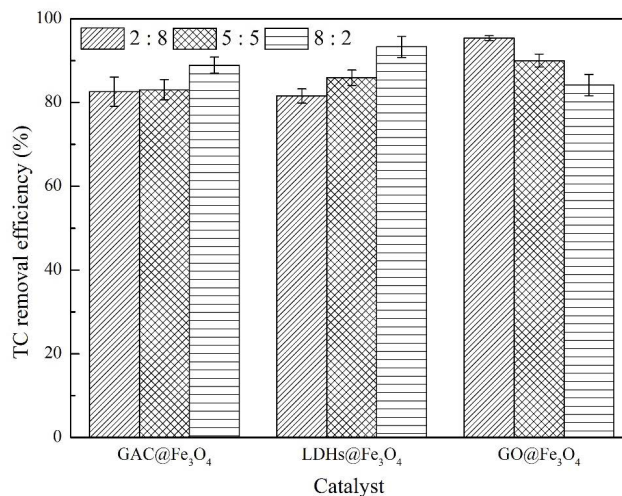


Fig. 6. TC-HCl removal efficiency with GAC@Fe<sub>3</sub>O<sub>4</sub>, LDHs@Fe<sub>3</sub>O<sub>4</sub> and GO@Fe<sub>3</sub>O<sub>4</sub> (pH = 3, air flow rate = 0.1 L min<sup>-1</sup>, current = 0.3 A, *t* = 2 h, and catalyst dosage = 1 g L<sup>-1</sup>).

as the proportion of Fe<sub>3</sub>O<sub>4</sub> content decreased, which were similar with the GAC@Fe<sub>3</sub>O<sub>4</sub>. Therefore, the ratio of the supporting materials and catalyst was 8:2 with pH of 3.

When GO was used as the supporting material, TC-HCl removal efficiencies were 95.37%, 90% and 84.15% with the mass ratios of 2:8, 5:5 and 8:2, respectively (Fig. 6). TC-HCl removal efficiency of the GO@Fe<sub>3</sub>O<sub>4</sub> was the highest compared with GAC and LDHs. Moreover, COD removal efficiencies were 60.69%, 48.4% and 42.11% when the mass ratios were 2:8, 5:5 and 8:2, respectively (Fig. 7c). Different from GAC and LDHs, when the mass ratio was 2:8, maximum COD removal efficiency was obtained. The reason may be that GO had rich functional groups on the surface and excellent conductivity comparing with GAC and LDHs [33], and the specific surface area of the supporting material was not the limiting factor of H<sub>2</sub>O<sub>2</sub> production, so COD removal efficiency increased with the increase of Fe<sub>3</sub>O<sub>4</sub>. Another reason might be that, enough H<sub>2</sub>O<sub>2</sub> reacted with •OH and •OH lost its ability to act as an EF reaction reagent [34]. Therefore, when the ratio of GO to Fe<sub>3</sub>O<sub>4</sub> was 8:2, the excessive H<sub>2</sub>O<sub>2</sub> lacked sufficient iron source, and a protonation reaction occurs instead. Obviously, when the mass ratio of the GO and Fe<sub>3</sub>O<sub>4</sub> was 2:8, TC-HCl and COD removal were the best at pH of 3.

Transition metal oxides had good catalytic activity in catalytic reactions. With the help of layered structure of LDHs, a kind of layered structured catalyst could be prepared. GAC had large specific surface area and developed pore structure. GO had huge specific surface area and good conductivity [12]. However, carbon materials also had shortcomings such as easy agglomeration and deactivation after long-term use, and easy oxidation under high current. Due to the dispersion of metal ions on the laminates of LDHs, LDH@Fe<sub>3</sub>O<sub>4</sub> used as catalyst had higher specific surface area and more active sites compared with GAC and GO. Therefore, compared with GAC and GO, LDHs used as a carrier had better performance in 3D-EF reaction. The ratio of supporting materials and Fe<sub>3</sub>O<sub>4</sub> also had a

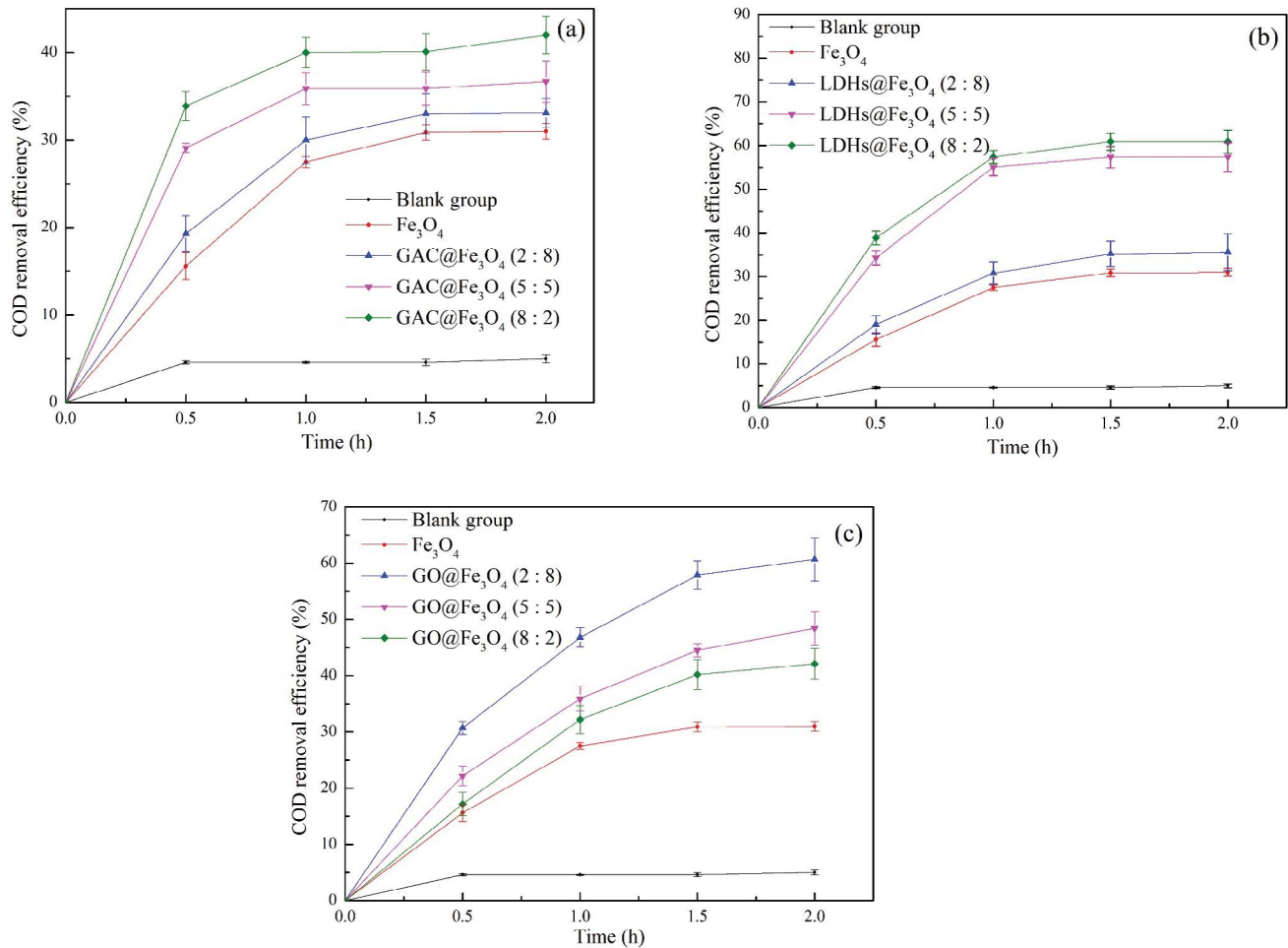


Fig. 7. COD removal efficiency with GAC@Fe<sub>3</sub>O<sub>4</sub> (a), LDHs@Fe<sub>3</sub>O<sub>4</sub> (b) and GO@Fe<sub>3</sub>O<sub>4</sub> (c) at different support materials/Fe<sub>3</sub>O<sub>4</sub> ratios (pH = 3, air flow rate = 0.1 L min<sup>-1</sup>, current = 0.3 A, *t* = 2 h, and catalyst dosage = 1 g L<sup>-1</sup>).

significant impact on the degradation effect. Theoretically, supporting materials had larger surface area, H<sub>2</sub>O<sub>2</sub> was easier to generate. Therefore, the larger the proportion of the supporting materials was, the better the organic pollutant removal performance would be. However, the iron content was also an important parameter. When GO was used as supporting material, due to its excellent electrical conductivity, the TC-HCl removal performance was better with the increasing iron content. However, the generation of H<sub>2</sub>O<sub>2</sub> would be suppressed with the increasing iron content, and peroxide precipitation was prone to produce.

### 3.3. Effect of pH value

The pH value was a key factor affecting the performance of the EF process at different levels of hydrogen peroxide and hydroxyl radicals, thereby affecting pollutant removal performance. Most of the studies on the EF process reported that the process showed better performance with pH value of around 3. However, the pH values of actual wastewater were always higher than 3, which had to be adjusted to ensure good performance of the EF [35]. Therefore, it was of great significance to study the effect of different pH values

on performance of the 3D-EF system. COD removal efficiencies at different pH values are shown in Fig. 8 using GAC@Fe<sub>3</sub>O<sub>4</sub> (8:2), LDHs@Fe<sub>3</sub>O<sub>4</sub> (8:2) and GO@Fe<sub>3</sub>O<sub>4</sub> (2:8) as catalyst particles.

As for GAC@Fe<sub>3</sub>O<sub>4</sub> (Fig. 8a), the highest COD removal efficiency was achieved at pH value of 3, and the lowest value was only 19.68% with pH of 9. In Fig. 8b, when LDHs@Fe<sub>3</sub>O<sub>4</sub> was selected as catalyst particles, the maximum COD removal efficiency of 63.03% was obtained with pH of 7, which was slightly higher than the COD removal efficiency at pH of 3. At different pH values, when LDHs@Fe<sub>3</sub>O<sub>4</sub> was used as catalyst, the system achieved excellent COD removal efficiency. The results showed that the LDHs were ideal supporting materials in the 3D-EF process. When the GO@Fe<sub>3</sub>O<sub>4</sub> was used as support material, with the increase of pH value, COD removal efficiency decreased obviously (Fig. 8c). The maximum COD removal efficiency of 60.69% was obtained with pH value of 3, which was still less than 63.03% of LDHs@Fe<sub>3</sub>O<sub>4</sub> at pH of 7. Obviously, using GAC@Fe<sub>3</sub>O<sub>4</sub> (8:2) and GO@Fe<sub>3</sub>O<sub>4</sub> (2:8) as catalyst particles, COD removal efficiencies of the 3D-EF system decreased as pH values increased. The results were similar with the research reported by Ganiyu et al. [36]. Under acidic conditions,

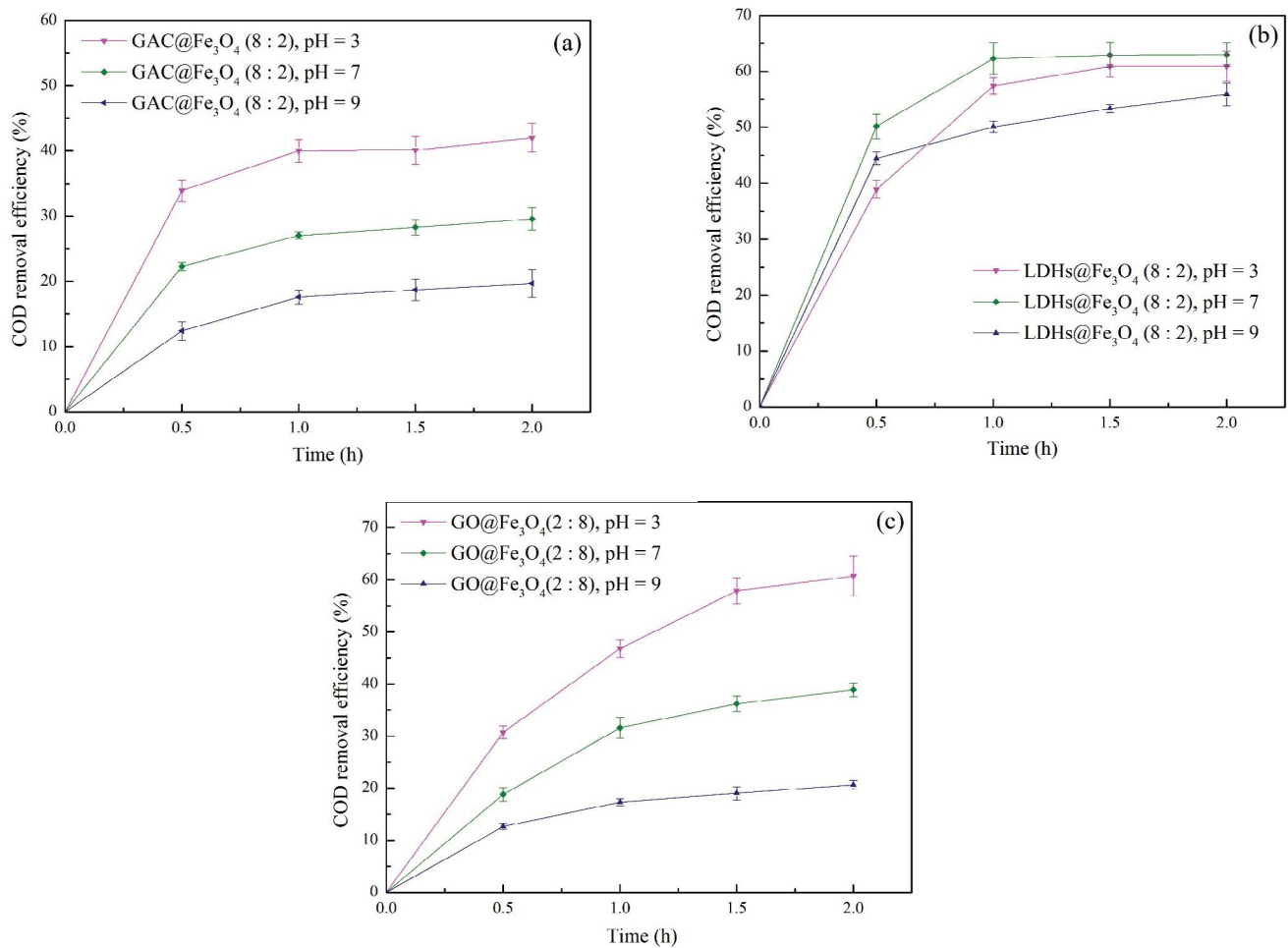


Fig. 8. COD removal efficiency with GAC@Fe<sub>3</sub>O<sub>4</sub> (a), LDHs@Fe<sub>3</sub>O<sub>4</sub> (b) and GO@Fe<sub>3</sub>O<sub>4</sub> (c) at different pH values (air flow rate = 0.1 L min<sup>-1</sup>, current = 0.3 A, *t* = 2 h, and catalyst dosage = 1 g L<sup>-1</sup>).

there was more H<sup>+</sup> in the solution, which would generate more H<sub>2</sub>O<sub>2</sub> and further more •OH. Using the LDHs@Fe<sub>3</sub>O<sub>4</sub> (8:2) as catalyst particles, COD removal efficiency at pH of 7 was higher than that at pH of 3. In fact, at neutral and alkaline pH values, the solubility of most iron catalysts was affected. The 3D-EF system could only be dominated by heterogeneous catalytic activation on the solid–liquid surface (Eqs. (1)–(3)), which was induced by the ≡Fe<sup>II</sup> and ≡Fe<sup>III</sup> species of bound iron present on the particles [37].



The reaction took place on the solid–liquid surface, and the surface catalysis process expanded the pH values range for the heterogeneous EF process without necessarily reducing the final removal efficiency. Therefore, the heterogeneous EF also showed good organic pollutant removal

effects under neutral or alkaline conditions. In this experiment, LDHs@Fe<sub>3</sub>O<sub>4</sub> (8:2) obtained the highest COD removal efficiency at pH of 7, which was much higher than that of GAC@Fe<sub>3</sub>O<sub>4</sub> (8:2) and GO@Fe<sub>3</sub>O<sub>4</sub> (2:8). The reason may be the case that the LDHs had a unique layered structure with large specific surface area. Fe<sub>3</sub>O<sub>4</sub> was embedded in the surface layer of LDHs. It was an integral part of the 3D-EF network. Compared with GAC@Fe<sub>3</sub>O<sub>4</sub> and GO@Fe<sub>3</sub>O<sub>4</sub>, the surface of LDHs@Fe<sub>3</sub>O<sub>4</sub> provided more exposed bound iron, which facilitated better COD removal performance. Besides, COD removal efficiency with the LDHs@Fe<sub>3</sub>O<sub>4</sub> (8:2) at pH of 7 was higher than that at pH of 3. This might be that LDHs was less stable under acidic conditions. At pH of 3, some Mg and Al were leached from the LDHs layered structure, and some Fe was leached from Fe<sub>3</sub>O<sub>4</sub>. Released ions such as Mg<sup>2+</sup>, Al<sup>3+</sup>, Fe<sup>2+</sup> and Fe<sup>3+</sup> were reprecipitated into LDHs possibly by reaction with intermediates. Therefore, the surface of the particle catalyst would be covered with some precipitates of impurities, and the active metal sites would be reduced, and organic pollutant removal efficiency would also be reduced. However, the dissolution of the LDHs was slight under neutral conditions, which was the reason that performance of LDHs@Fe<sub>3</sub>O<sub>4</sub> was the

best with pH of 7. Studies obtained a similar conclusion as well [38]. In summary, COD removal performance of the 3D-EF system with GAC@Fe<sub>3</sub>O<sub>4</sub> and GO@Fe<sub>3</sub>O<sub>4</sub> was greatly affected by pH values while LDHs@Fe<sub>3</sub>O<sub>4</sub> were less affected, which was suitable for practical application.

Both LDHs and GO were excellent catalyst supporting materials. According to the results of TC-HCl removal, LDHs@Fe<sub>3</sub>O<sub>4</sub> (8:2) and GO@Fe<sub>3</sub>O<sub>4</sub> (2:8) had better TC-HCl removal efficiencies at pH of 3. However, LDHs@Fe<sub>3</sub>O<sub>4</sub> (8:2) were unstable under acidic conditions, which reduced the active potential of the catalyst. As for GO@Fe<sub>3</sub>O<sub>4</sub> (2:8), at pH of 3, the surface O<sub>2</sub> also had more four-electron transfer reactions at the same time (Eq. (4)), which was not conducive to the production of H<sub>2</sub>O<sub>2</sub>, so the removal efficiency was also suppressed. Therefore, the performance of LDHs@Fe<sub>3</sub>O<sub>4</sub> (8:2) and GO@Fe<sub>3</sub>O<sub>4</sub> (2:8) was similar at pH of 3.



Under acidic conditions, there were plenty of H<sup>+</sup> in the solution, and more H<sub>2</sub>O<sub>2</sub> would be produced comparing with alkaline conditions. More iron on the surface of the catalyst could participate in the 3D-EF reaction in acidic conditions, so the 3D-EF reaction was strengthened and more •OH was produced. In addition, •OH had strong oxidation potential and high oxidation efficiency under acidic conditions. Under alkaline conditions, the amount of H<sub>2</sub>O<sub>2</sub> produced was less than in the acidic environment, and the produced H<sub>2</sub>O<sub>2</sub> was readily decomposed into H<sub>2</sub>O and O<sub>2</sub>, which hindered the production of •OH. In addition, under alkaline conditions, iron species were prone to precipitate in the form of iron hydroxide. Therefore, the performance of the 3D-EF system under acidic conditions was significantly better than in alkaline environment.

### 3.4. Ferrous iron concentration in the solution

The most important performance requirements of efficient heterogeneous catalysts included that the catalysts maintained catalytic activity and stability under a wide range of experimental conditions. Studies have

shown that the most existing catalysts underwent obvious leaching under strong acid conditions, making the system exhibit both homogeneous and heterogeneous EF processes. But this situation should be avoided because it would exhaust the active metal sites of the solid catalyst and reduce repeatability [39]. Ferrous iron (Fe<sup>2+</sup>) concentration in the solution of the three catalyst particles at the optimal mass ratio with pH of 7 is shown in Fig. 9a.

Fe<sup>2+</sup> concentration in the solution followed the sequence, LDHs@Fe<sub>3</sub>O<sub>4</sub> (8:2) < GAC@Fe<sub>3</sub>O<sub>4</sub> (8:2) < GO@Fe<sub>3</sub>O<sub>4</sub> (2:8). Fe<sup>2+</sup> concentration in the solution of the GO@Fe<sub>3</sub>O<sub>4</sub> was 2.62 mg L<sup>-1</sup>, much higher than the other two, which showed the iron loss of the GO@Fe<sub>3</sub>O<sub>4</sub> (2:8) was serious although the amount of Fe<sub>3</sub>O<sub>4</sub> on the GO was originally high. As was shown in Fig. 9b, the percentage of Fe<sup>2+</sup> leaching to solution of GO@Fe<sub>3</sub>O<sub>4</sub> was 5.46%, which was the highest. Therefore, using GO@Fe<sub>3</sub>O<sub>4</sub> as the catalyst particle, two processes, homogeneous EF in solution and heterogeneous oxidation on solid–liquid surface, occurred in the 3D-EF system. The contribution of homogeneous EF decreased with the increase of pH values. In contrast, when the LDHs@Fe<sub>3</sub>O<sub>4</sub> was used as the catalyst particles, the iron loss was the least among the three particles after the reaction, which indicated that the LDHs@Fe<sub>3</sub>O<sub>4</sub> was a perfect support material for the 3D-EF process. Using the GAC@Fe<sub>3</sub>O<sub>4</sub> as catalyst particle, the iron loss was also less, so only heterogeneous oxidation on solid–liquid surface happened in the system, and the homogeneous EF was negligible. Moreover, Fe<sup>2+</sup> concentration in the LDHs@Fe<sub>3</sub>O<sub>4</sub> supported 3D-EF increased first and then decreased as the reaction proceeded. The reason might be that with the removal of TC-HCl, the iron ions in the solution returned to the surface of the LDH@Fe<sub>3</sub>O<sub>4</sub>, or the oxidation of ferrous ion by H<sub>2</sub>O<sub>2</sub>/•OH remaining in solution to ferric ions [40]. The results indicated that the LDHs had the best ability to keep the catalyst among the three particles.

### 3.5. H<sub>2</sub>O<sub>2</sub> and •OH concentrations

H<sub>2</sub>O<sub>2</sub> and •OH concentrations were direct indicators reflecting removal performance of the EF process. At pH of 7,

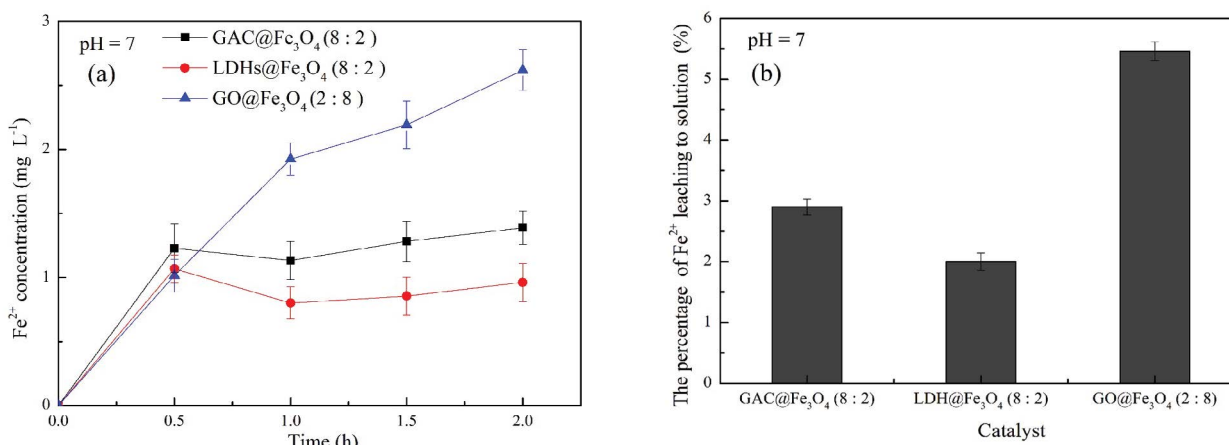


Fig. 9. Fe<sup>2+</sup> concentration in the three catalyst particles supplied 3D-EF system at the best mass ratios (a) and the percentage of Fe<sup>2+</sup> leaching to solution (b) (pH = 7, air flow rate = 0.1 L min<sup>-1</sup>, current = 0.3 A, t = 2 h, and catalyst dosage = 1 g L<sup>-1</sup>).

when the three catalyst particles were composed in different ratios, COD removal efficiencies were mostly similar to that at pH of 3. At pH of 7, the relationship between COD removal efficiency and the  $\text{H}_2\text{O}_2$  and  $\cdot\text{OH}$  concentrations was studied. The  $\text{H}_2\text{O}_2$  and  $\cdot\text{OH}$  concentrations in the solution after 2 h of reaction are shown in Figs. 10a and b, respectively.

The results in Fig. 10 showed that  $\text{H}_2\text{O}_2$  and  $\cdot\text{OH}$  concentrations were consistent with COD removal efficiencies. The higher the  $\cdot\text{OH}$  concentration was, the greater the COD removal efficiency obtained, indicating that  $\cdot\text{OH}$  was the main active species during the EF process. During the Fenton oxidation process,  $\text{H}_2\text{O}_2$  played an important role in the generation of  $\cdot\text{OH}$ . In Fig. 10b, the results showed a positive correlation between  $\cdot\text{OH}$  concentration and  $\text{H}_2\text{O}_2$  concentration. A large number of studies had shown that COD removal efficiency increased with the increasing  $\text{H}_2\text{O}_2$  concentration, but the efficiency would decrease after reaching a peak value [41]. The maximum COD removal efficiency was obtained with LDHs@ $\text{Fe}_3\text{O}_4$  (8:2) at pH of 7. Obviously, the system of the LDHs@ $\text{Fe}_3\text{O}_4$  (8:2) had the highest  $\text{H}_2\text{O}_2$  concentration ( $0.031 \text{ mol L}^{-1}$ ) and  $\cdot\text{OH}$  concentration ( $0.26 \text{ mmol L}^{-1}$ ). In fact, the MgAl-LDHs had required structural characteristics and elemental composition for promoting heterogeneous EF reaction. The schematic representation of the LDHs@ $\text{Fe}_3\text{O}_4$  is proposed by Fig. 11. The LDHs@ $\text{Fe}_3\text{O}_4$  maintained stability under neutral condition, the 3D-EF could generate more  $\cdot\text{OH}$  and achieve better catalytic effects.

### 3.6. Possible pathway of TC removal

The possible products during the degradation of TC-HCl were identified by GC-MS. Fig. S3 shows the chromatogram of TC-HCl degradation with GAC@ $\text{Fe}_3\text{O}_4$  (a), GO@ $\text{Fe}_3\text{O}_4$  (b) and LDHs@ $\text{Fe}_3\text{O}_4$  (c). Table S1 shows the main intermediates during the 3D-EF process. The intermediate compounds obtained by the three catalysts were similar. The results indicated that the degradation mechanisms of the TC-HCl were almost the same with different types of supporting materials.  $\text{O}_2$  obtained electrons on the surface of the cathode, and reacted to produce  $\text{H}_2\text{O}_2$ .  $\text{H}_2\text{O}_2$  continued to react

with the iron ion to produce  $\cdot\text{OH}$ . Finally,  $\cdot\text{OH}$  reacted with TC-HCl to generate various intermediate compounds, and some intermediate compounds were completely degraded into  $\text{CO}_2$  and  $\text{H}_2\text{O}$ .

The major intermediates were identified to be organic acids, such as oxalic acid, acetic acid, which was consistent with previous report [42]. High electron density would make the functional group an easy target for  $\cdot\text{OH}$  attacking in the EF process. There were three typical functional groups in TC-HCl, double bonds ( $\text{C}_{11a}-\text{C}_{12}$  (higher) and  $\text{C}_2-\text{C}_3$ ), amine group and phenolic group [43]. The structure diagram of TC-HCl is shown in Fig. 12. The  $\text{C}_{11a}-\text{C}_{12}$  double bond has been reported to be the most reactive position to be attacked by  $\cdot\text{OH}$ . Next was  $\text{C}_2-\text{C}_3$  double bond. Then a series of the ring-opening reaction ( $\text{C}_{6a}-\text{C}_7$ ) and alternate attack reaction ( $\text{C}_6, \text{C}_4, \text{C}_{10}-\text{C}_{10a}$ ) reacted to final production of inorganic ions,  $\text{CO}_2$  and  $\text{H}_2\text{O}$  [44].

## 4. Conclusions

Antibiotic pollution has become a focus of public attention. Compared with GO and GAC, MgAl-LDHs had a more obvious advantage in removing TC-HCl in water as a supporting material for the 3D-EF process. The COD

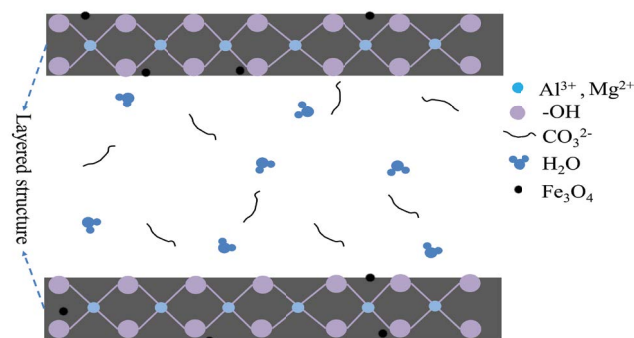


Fig. 11. Schematic representation of the LDHs@ $\text{Fe}_3\text{O}_4$ .

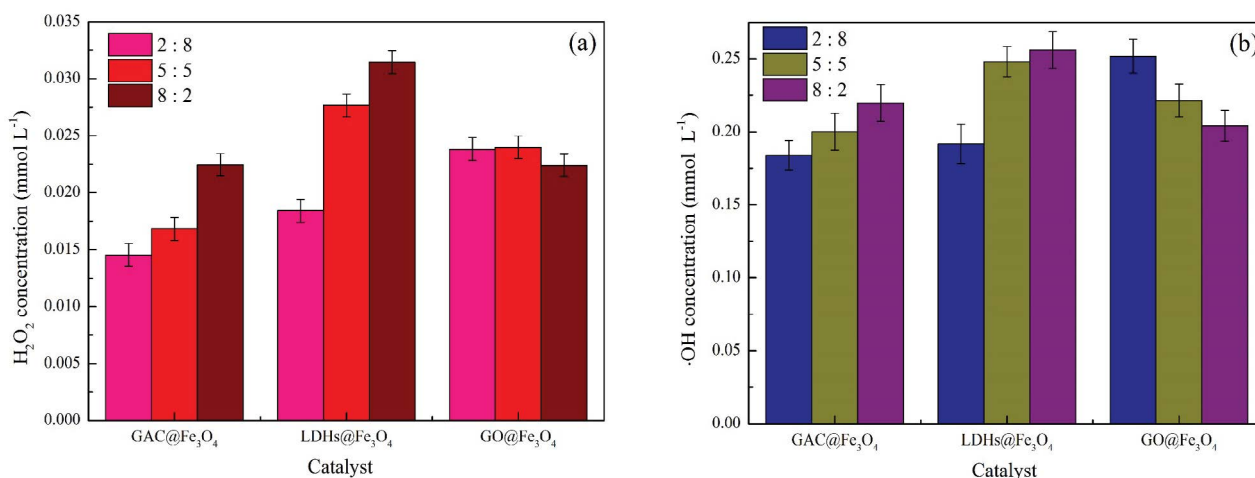


Fig. 10.  $\text{H}_2\text{O}_2$  concentration (a) and  $\cdot\text{OH}$  concentration (b) of three proportion of GAC@ $\text{Fe}_3\text{O}_4$ , LDHs@ $\text{Fe}_3\text{O}_4$  and GO@ $\text{Fe}_3\text{O}_4$  at pH of 7 (air flow rate =  $0.1 \text{ L min}^{-1}$ , current =  $0.3 \text{ A}$ ,  $t = 2 \text{ h}$ , and catalyst dosage =  $1 \text{ g L}^{-1}$ ).

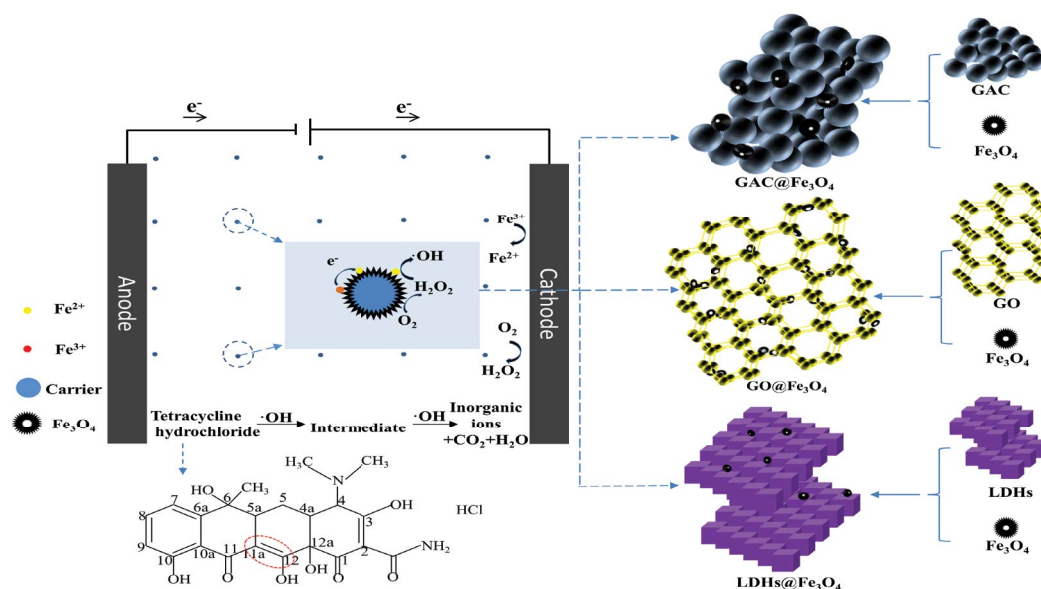


Fig. 12. Demonstration diagram of 3D-EF removal of TC-HCl.

removal efficiency of LDHs@Fe<sub>3</sub>O<sub>4</sub> (8:2) was the highest under the three types of catalysts and the three ratios, which was due to the higher specific surface area and more active sites of the LDHs. When GAC@Fe<sub>3</sub>O<sub>4</sub> and LDHs@Fe<sub>3</sub>O<sub>4</sub> were used as catalysts, COD removal efficiency increased as the proportion of support materials increased due to the generation of H<sub>2</sub>O<sub>2</sub> on the surface of the supporting materials. Because of rich functional groups on the surface and stronger conductive ability of GO, COD removal efficiencies increased with the increase of the ratio of Fe<sub>3</sub>O<sub>4</sub>. In addition, when GAC@Fe<sub>3</sub>O<sub>4</sub> (8:2) and GO@Fe<sub>3</sub>O<sub>4</sub> (2:8) were used as catalysts, COD removal efficiency decreased with increasing pH, this was because that more H<sub>2</sub>O<sub>2</sub> could be produced under acidic conditions, more iron ion could participate in the 3D-EF reaction, and  $\cdot\text{OH}$  had stronger oxidation potential under acidic conditions. COD removal efficiency of the LDHs@Fe<sub>3</sub>O<sub>4</sub> (8:2) was the highest at pH of 7. This was because LDHs rarely dissolved Mg, Al and Fe ions under neutral conditions, which prevented these ions from reacting with some pollutant intermediates to form precipitate and to cover the surface of the catalyst. The conclusion could be demonstrated by the following aspects: (1) ferrous ion of the LDHs@Fe<sub>3</sub>O<sub>4</sub> had the least dissolution (2%) under neutral conditions compared with the GAC@Fe<sub>3</sub>O<sub>4</sub> (2.9%) and GO@Fe<sub>3</sub>O<sub>4</sub> (5.46%). (2) According to the characterization results of the XRD, EDS, SEM, FTIR, XPS and BET, the LDHs@Fe<sub>3</sub>O<sub>4</sub> had a layered structure and a larger specific surface area compared with the other two materials. (3) LDHs@Fe<sub>3</sub>O<sub>4</sub> (8:2) as the catalyst, the concentrations of H<sub>2</sub>O<sub>2</sub> (0.031 mmol L<sup>-1</sup>) and  $\cdot\text{OH}$  (0.26 mmol L<sup>-1</sup>) were the highest under neutral conditions. Therefore, the LDHs@Fe<sub>3</sub>O<sub>4</sub> were high-quality catalyst particles for the 3D-EF process.

### Acknowledgments

This research was supported by the International Scientific and Technological Innovation and Cooperation Project of Sichuan (No. 2019YFH0170).

### References

- [1] M. Wang, L. Zhang, G. Zhang, T. Pang, X. Zhang, D. Cai, Z. Wu, In situ degradation of antibiotic residues in medical intravenous infusion bottles using high energy electron beam irradiation, *Sci. Rep.*, 7 (2017) 39928.
- [2] I. Sires, E. Brillas, Remediation of water pollution caused by pharmaceutical residues based on electrochemical separation and degradation technologies: a review, *Environ. Int.*, 40 (2012) 212–229.
- [3] Y. Sun, W. Zheng, S. Fu, R.P. Singh, Immobilization of iron phthalocyanine on 4-aminopyridine grafted polystyrene resin as a catalyst for peroxymonosulfate activation in eliminating tetracycline hydrochloride, *Chem. Eng. J.*, 391 (2020) 123611.
- [4] H.U. Rasheed, X. Lv, S. Zhang, W. Wei, N. ullah, J. Xie, Ternary MIL-100(Fe)@Fe<sub>3</sub>O<sub>4</sub>/CA magnetic nanophotocatalysts (MNPCs): magnetically separable and Fenton-like degradation of tetracycline hydrochloride, *Adv. Powder Technol.*, 29 (2018) 3305–3314.
- [5] J. De Coster, W. Vanherck, L. Appels, R. Dewil, Selective electrochemical degradation of 4-chlorophenol at a Ti/RuO<sub>2</sub>-IrO<sub>2</sub> anode in chloride rich wastewater, *J. Environ. Manage.*, 190 (2017) 61–71.
- [6] V. Poza-Nogueiras, E. Rosales, M. Pazos, M.A. Sanroman, Current advances and trends in electro-Fenton process using heterogeneous catalysts - a review, *Chemosphere*, 201 (2018) 399–416.
- [7] A. Babuponnusami, K. Muthukumar, A review on Fenton and improvements to the Fenton process for wastewater treatment, *J. Environ. Chem. Eng.*, 2 (2014) 557–572.
- [8] L. Xu, J. Wang, Fenton-like degradation of 2,4-dichlorophenol using Fe<sub>3</sub>O<sub>4</sub> magnetic nanoparticles, *Appl. Catal. B*, 123–124 (2012) 117–126.
- [9] F. Ghanbari, C.A. Martínez-Huitle, Electrochemical advanced oxidation processes coupled with peroxymonosulfate for the treatment of real washing machine effluent: a comparative study, *J. Electroanal. Chem.*, 847 (2019) 113182.
- [10] I.M. Ahmed, M.S. Gasser, Adsorption study of anionic reactive dye from aqueous solution to Mg-Fe-CO<sub>3</sub> layered double hydroxide (LDH), *Appl. Surf. Sci.*, 259 (2012) 650–656.
- [11] Y. Huang, Y. Yang, X. Wang, X. Yuan, N. Pi, H. Yuan, X. Liu, C. Ni, Heterogeneous Fenton-like degradation of methoxychlor in water using two different FeS@hydroxalites (LHDs) and Fe<sub>3</sub>O<sub>4</sub>@LHDs catalysts prepared via an in situ growth method, *Chem. Eng. J.*, 342 (2018) 142–154.

- [12] N. Fernández-Sáez, D.E. Villela-Martinez, F. Carrasco-Marín, A.F. Pérez-Cadenas, L.M. Pastrana-Martínez, Heteroatom-doped graphene aerogels and carbon-magnetite catalysts for the heterogeneous electro-Fenton degradation of acetaminophen in aqueous solution, *J. Catal.*, 378 (2019) 68–79.
- [13] C. Sun, S.-T. Yang, Z. Gao, S. Yang, A. Yilihamu, Q. Ma, R.-S. Zhao, F. Xue,  $\text{Fe}_3\text{O}_4/\text{TiO}_2$ /reduced graphene oxide composites as highly efficient Fenton-like catalyst for the decoloration of methylene blue, *Mater. Chem. Phys.*, 223 (2019) 751–757.
- [14] A. Wang, J. Qu, J. Ru, H. Liu, J. Ge, Mineralization of an azo dye Acid Red 14 by electro-Fenton's reagent using an activated carbon fiber cathode, *Dyes Pigm.*, 65 (2005) 227–233.
- [15] B. Bektasoglu, M. Ozyurek, K. Guclu, R. Apak, Hydroxyl radical detection with a salicylate probe using modified CUPRAC spectrophotometry and HPLC, *Talanta*, 77 (2008) 90–97.
- [16] H.T. Van, L.H. Nguyen, T.K. Hoang, T.T. Nguyen, T.N.H. Tran, T.B.H. Nguyen, X.H. Vu, M.T. Pham, T.P. Tran, T.T. Pham, H.D. Nguyen, H.-P. Chao, C.-C. Lin, X.C. Nguyen, Heterogeneous Fenton oxidation of paracetamol in aqueous solution using iron slag as a catalyst: degradation mechanisms and kinetics, *Environ. Technol. Innov.*, 18 (2020) 100670.
- [17] M. Ghasemi, A. Khataee, P. Gholami, R.D. Cheshmeh Soltani, Template-free microspheres decorated with Cu-Fe-NLDH for catalytic removal of gentamicin in heterogeneous electro-Fenton process, *J. Environ. Manage.*, 248 (2019) 109236.
- [18] L. Adlnasab, M. Ezoddin, M.A. Karimi, N. Hatamikia, MCM-41@Cu-Fe-LDH magnetic nanoparticles modified with cationic surfactant for removal of Alizarin Yellow from water samples and its determination with HPLC, *Res. Chem. Intermed.*, 44 (2018) 3249–3265.
- [19] Z. Wu, X. Yuan, H. Zhong, H. Wang, L. Jiang, G. Zeng, H. Wang, Z. Liu, Y. Li, Highly efficient adsorption of Congo red in single and binary water with cationic dyes by reduced graphene oxide decorated  $\text{NH}_2$ -MIL-68(Al), *J. Mol. Liq.*, 247 (2017) 215–229.
- [20] X. Wu, B. Li, X. Wen, Synthesis and adsorption properties of hierarchical  $\text{Fe}_3\text{O}_4$ @MgAl-LDH magnetic microspheres, *J. Nanopart. Res.*, 19 (2017) 131.
- [21] R. Han, W. Li, W. Pan, M. Zhu, D. Zhou, F.-s. Li, 1D Magnetic Materials of  $\text{Fe}_3\text{O}_4$  and Fe with high performance of microwave absorption fabricated by electrospinning method, *Sci. Rep.*, 4 (2014) 7493.
- [22] K. Morimoto, K. Tamura, H. Yamada, T. Sato, M. Suzuki, Determination and reduction of Fe(III) incorporated into Mg-Fe layered double hydroxide structures, *Appl. Clay Sci.*, 121–122 (2016) 71–76.
- [23] L. Adlnasab, N. Shekari, A. Maghsodi, Optimization of arsenic removal with  $\text{Fe}_3\text{O}_4$ @ $\text{Al}_2\text{O}_3$ @Zn-Fe LDH as a new magnetic nano adsorbent using Box-Behnken design, *J. Environ. Chem. Eng.*, 7 (2019) 102974.
- [24] G. Zeng, Y. Liu, L. Tang, G. Yang, Y. Pang, Y. Zhang, Y. Zhou, Z. Li, M. Li, M. Lai, X. He, Y. He, Enhancement of Cd(II) adsorption by polyacrylic acid modified magnetic mesoporous carbon, *Chem. Eng. J.*, 259 (2015) 153–160.
- [25] Y.-J. Lin, D.-Q. Li, D.G. Evans, X. Duan, Modulating effect of Mg-Al- $\text{CO}_3$  layered double hydroxides on the thermal stability of PVC resin, *Polym. Degrad. Stab.*, 88 (2005) 286–293.
- [26] J. Ni, J. Xue, L. Xie, J. Shen, G. He, H. Chen, Construction of magnetically separable NiAl LDH/ $\text{Fe}_3\text{O}_4$ -RGO nanocomposites with enhanced photocatalytic performance under visible light, *Phys. Chem. Phys.*, 20 (2018) 414–421.
- [27] Y. Xie, X. Yuan, Z. Wu, G. Zeng, L. Jiang, X. Peng, H. Li, Adsorption behavior and mechanism of Mg/Fe layered double hydroxide with  $\text{Fe}_3\text{O}_4$ -carbon spheres on the removal of Pb(II) and Cu(II), *J. Colloid Interface Sci.*, 536 (2019) 440–455.
- [28] N. Chubar, V. Gerda, O. Megantari, M. Mičušík, M. Omastova, K. Heister, P. Man, J. Fraissard, Applications versus properties of Mg-Al layered double hydroxides provided by their syntheses methods: alkoxide and alkoxide-free sol-gel syntheses and hydrothermal precipitation, *Chem. Eng. J.*, 234 (2013) 284–299.
- [29] X.Y. Chen, B.H. Liu, Z.P. Li,  $\text{Fe}_3\text{O}_4/\text{C}$  composites synthesized from Fe-based xerogels for anode materials of Li-ion batteries, *Solid State Ionics*, 261 (2014) 45–52.
- [30] Y. Guo, Z. Gong, C. Li, B. Gao, P. Li, X. Wang, B. Zhang, X. Li, Efficient removal of uranium (VI) by 3D hierarchical Mg/Fe-LDH supported nanoscale hydroxyapatite: a synthetic experimental and mechanism studies, *Chem. Eng. J.*, 392 (2020) 123682.
- [31] P. Salimi, O. Norouzi, S.E.M. Pourhosseini, Two-step synthesis of nanohusk  $\text{Fe}_3\text{O}_4$  embedded in 3D network pyrolytic marine biochar for a new generation of anode materials for Lithium-Ion batteries, *J. Alloys Compd.*, 786 (2019) 930–937.
- [32] N. Wang, T. Zheng, G. Zhang, P. Wang, A review on Fenton-like processes for organic wastewater treatment, *J. Environ. Chem. Eng.*, 4 (2016) 762–787.
- [33] A.T. Smith, A.M. LaChance, S. Zeng, B. Liu, L. Sun, Synthesis, properties, and applications of graphene oxide/reduced graphene oxide and their nanocomposites, *Nano Mater. Sci.*, 1 (2019) 31–47.
- [34] S.O. Ganiyu, M. Zhou, C.A. Martínez-Huitle, Heterogeneous electro-Fenton and photoelectro-Fenton processes: a critical review of fundamental principles and application for water/wastewater treatment, *Appl. Catal. B*, 235 (2018) 103–129.
- [35] E. Brillas, S. Garcia-Segura, Benchmarking recent advances and innovative technology approaches of Fenton, photo-Fenton, electro-Fenton, and related processes: a review on the relevance of phenol as model molecule, *Sep. Purif. Technol.*, 237 (2020) 116337.
- [36] S.O. Ganiyu, T.X. Huong Le, M. Bechelany, N. Oturan, S. Papirio, G. Esposito, E. van Hullebusch, M. Cretin, M.A. Oturan, Electrochemical mineralization of sulfamethoxazole over wide pH range using FeII/FeIII LDH modified carbon felt cathode: degradation pathway, toxicity and reusability of the modified cathode, *Chem. Eng. J.*, 350 (2018) 844–855.
- [37] Y. Zhu, R. Zhu, Y. Xi, J. Zhu, G. Zhu, H. He, Strategies for enhancing the heterogeneous Fenton catalytic reactivity: a review, *Appl. Catal. B*, 255 (2019) 117739.
- [38] P. Zhong, Q. Yu, J. Zhao, S. Xu, X. Qiu, J. Chen, Degradation of bisphenol A by Fe-Al layered double hydroxides: a new synergy of homo- and heterogeneous Fenton systems, *J. Colloid Interface Sci.*, 552 (2019) 122–133.
- [39] W. Qiao, H. Bai, T. Tang, J. Miao, Q. Yang, Recovery and utilization of phosphorus in wastewater by magnetic  $\text{Fe}_3\text{O}_4$ /Zn-Al-Fe-La layered double hydroxides(LDHs), *Colloids Surf., A*, 577 (2019) 118–128.
- [40] Q. Wang, S. Tian, J. Long, P. Ning, Use of Fe(II)Fe(III)-LDHs prepared by co-precipitation method in a heterogeneous-Fenton process for degradation of Methylene Blue, *Catal. Today*, 224 (2014) 41–48.
- [41] J. Casado, Towards industrial implementation of Electro-Fenton and derived technologies for wastewater treatment: a review, *J. Environ. Chem. Eng.*, 7 (2019) 102823.
- [42] Y. Zhang, S. Zuo, M. Zhou, L. Liang, G. Ren, Removal of tetracycline by coupling of flow-through electro-Fenton and in-situ regenerative active carbon felt adsorption, *Chem. Eng. J.*, 335 (2018) 685–692.
- [43] L. Tang, C. Feng, Y. Deng, G. Zeng, J. Wang, Y. Liu, H. Feng, J. Wang, Enhanced photocatalytic activity of ternary  $\text{Ag/g-C}_3\text{N}_4/\text{NaTaO}_3$  photocatalysts under wide spectrum light radiation: the high potential band protection mechanism, *Appl. Catal. B*, 230 (2018) 102–114.
- [44] T. Luo, H. Feng, L. Tang, Y. Lu, W. Tang, S. Chen, J. Yu, Q. Xie, X. Ouyang, Z. Chen, Efficient degradation of tetracycline by heterogeneous electro-Fenton process using Cu-doped  $\text{Fe}@\text{Fe}_3\text{O}_4$ : mechanism and degradation pathway, *Chem. Eng. J.*, 382 (2020) 122970.

## Supplementary information:

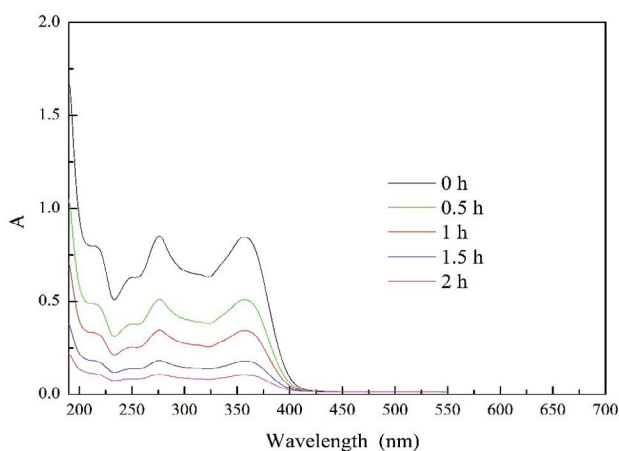


Fig. S1. TC-HCl degradation with LDHs@Fe<sub>3</sub>O<sub>4</sub> (8:2) in different electrolysis time (pH = 3, air flow rate = 0.1 L min<sup>-1</sup>, current = 0.3 A, *t* = 2 h, catalyst dosage = 1 g L<sup>-1</sup>, and water sample was diluted four times).

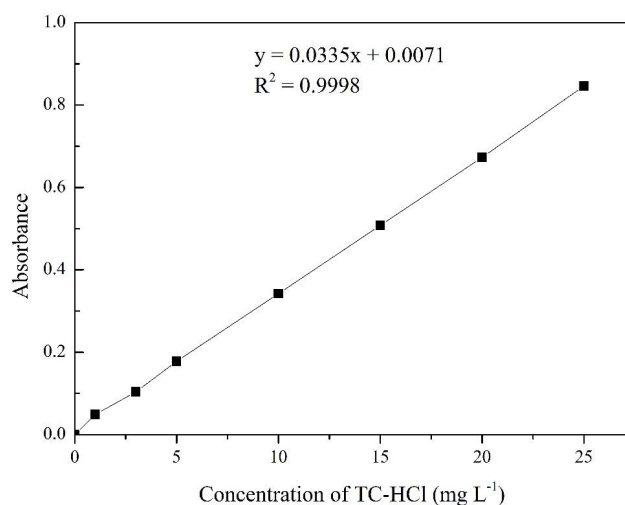


Fig. S2. Standard curve of TC-HCl by a UV-vis spectrophotometer.

Table S1

Possible degradation intermediates identified by GC-MS

Compound	Molecular formula	Retention time (min)	Molecular mass (g mol <sup>-1</sup> )	Molecular structure
1	C <sub>4</sub> H <sub>10</sub> O	1.109	74	
2	C <sub>5</sub> H <sub>10</sub> O <sub>2</sub>	2.277	102	
3	C <sub>2</sub> NH <sub>3</sub> O	6.055	59	
4	C <sub>2</sub> H <sub>4</sub> O <sub>2</sub>	15.424	60	
5	C <sub>5</sub> H <sub>12</sub> O <sub>2</sub>	18.081	104	
6	C <sub>10</sub> O <sub>2</sub> H <sub>14</sub>	19.461	166	
7	C <sub>7</sub> H <sub>14</sub> O	20.000	114	
8	C <sub>8</sub> H <sub>18</sub> O	21.428	130	
9	C <sub>9</sub> H <sub>18</sub> O	21.556	142	
10	C <sub>6</sub> H <sub>12</sub> O	21.835	100	
11	C <sub>2</sub> O <sub>4</sub> H <sub>2</sub>	27.866	90	
12	C <sub>9</sub> H <sub>10</sub> O	28.535	134	

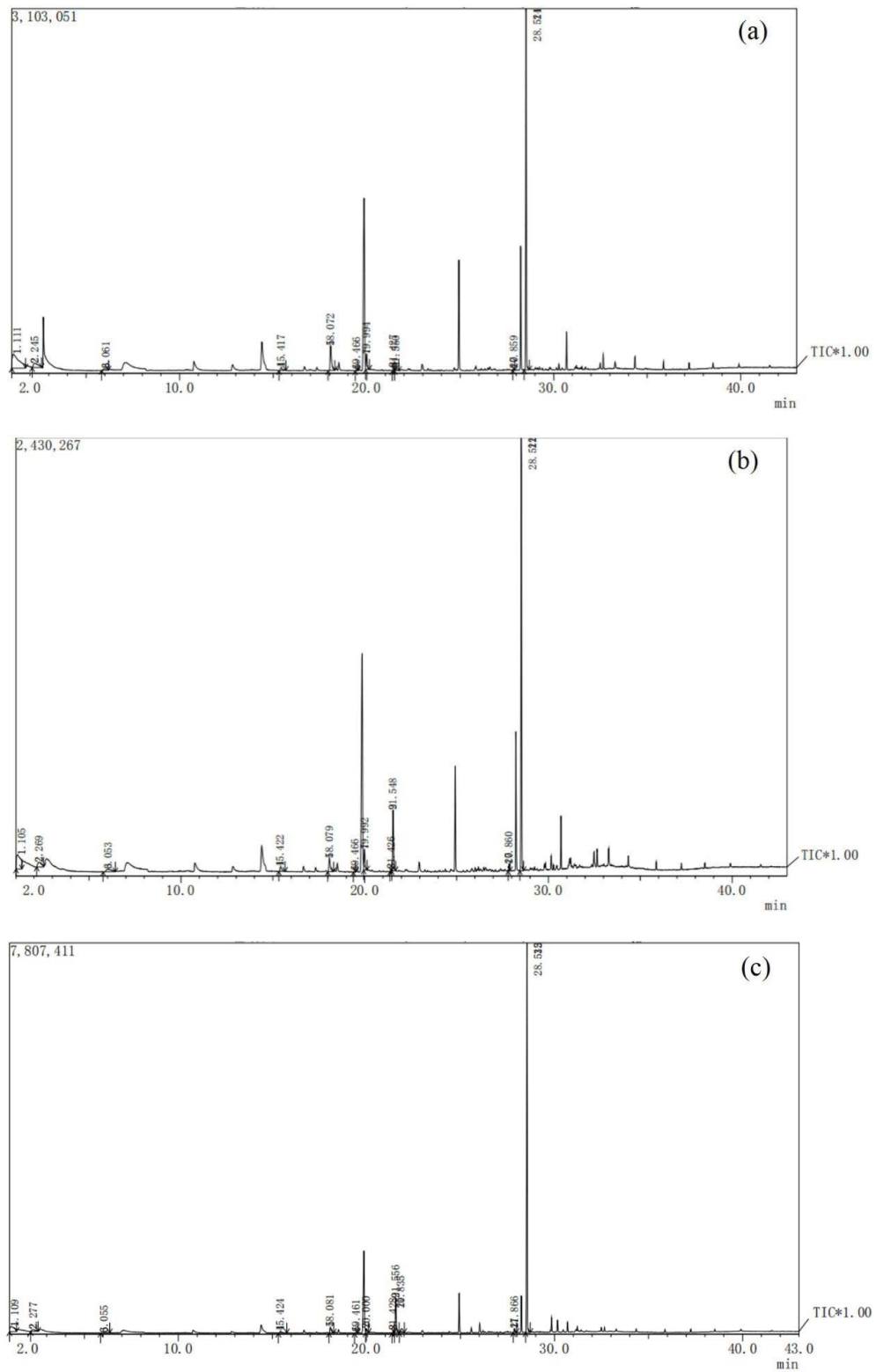


Fig. S3. Chromatogram of TC-HCl degradation with GAC@Fe<sub>3</sub>O<sub>4</sub> (a), GO@Fe<sub>3</sub>O<sub>4</sub> (b) and LDHs@Fe<sub>3</sub>O<sub>4</sub> (c).